Taylor & Francis
Taylor & Francis Group

Combustion Science and Technology

ISSN: 0010-2202 (Print) 1563-521X (Online) Journal homepage: https://www.tandfonline.com/loi/gcst20

Self-sustained CO Combustion Induced by $CuCe_{0.75}Zr_{0.25}O_y$ Catalysts with Different Pore-forming Methods

Junyao He, Running Kang, Qing Zhang, Xiaolin Wei, Baojuan Dou & Feng Bin

To cite this article: Junyao He, Running Kang, Qing Zhang, Xiaolin Wei, Baojuan Dou & Feng Bin (2020): Self-sustained CO Combustion Induced by $CuCe_{0.75}Zr_{0.25}O_y$ Catalysts with Different Pore-forming Methods, Combustion Science and Technology, DOI: 10.1080/00102202.2020.1727455

To link to this article: https://doi.org/10.1080/00102202.2020.1727455

COMBUSTION SCIENCE AND TECHNOLOGY
https://doi.org/10.1080/00102202.2020.1727455

Taylor & Francis
Taylor & Francis Group

Self-sustained CO Combustion Induced by $CuCe_{0.75}Zr_{0.25}O_y$ Catalysts with Different Pore-forming Methods

Junyao He[a,b], Running Kang[a,c], Qing Zhang[d], Xiaolin Wei[a,c], Baojuan Dou[d], and Feng Bin[a]

[a]State Key Laboratory of High-Temperature Gas Dynamics, Institute of Mechanics, Chinese Academy of Sciences, Beijing, PR China; [b]School of Energy and Power Engineering, Xi'an Jiaotong University, Xi'an, PR China; [c]School of Engineering Science, University of Chinese Academy of Sciences, Beijing, PR China; [d]College of Chemical Engineering & Materials Science, Tianjin University of Science & Technology, Tianjin, PR China

ABSTRACT

CO self-sustaining combustion, induced by a $CuCe_{0.75}Zr_{0.25}O_y$ catalyst, has been confirmed experimentally as an effective strategy to reduce serious environmental pollution and energy waste, which is caused by direct combustion of conventional converter gas in the steelmaking industry. In this paper, the effects of $CuCe_{0.75}Zr_{0.25}O_y$ catalysts prepared by a sol-gel method via three different pore-forming agents (oxalic acid, cellulose and thermal decomposition) were investigated for their catalytic activity of self-sustained CO combustion. Additionally, characterization methods were used to obtain the structural properties of each catalyst. The results obtained show that the $CuCe_{0.75}Zr_{0.25}O_y$ catalyst, as a sol-gel pore-forming agent, prepared from cellulose exhibits the highest activity among the three catalysts. Under the condition of a reaction gas (3% CO+5% O_2/N_2), the T_{10} (70°C), T_{50} (73°C) and T_{90} (78°C) of the cellulose catalyst are obviously lower than those of the other catalysts, where T_{10}, T_{50} and T_{90} denote the reaction temperature corresponding to the CO conversion of 10%, 50% and 90%, respectively. The reason is that the cellulose pore-forming agent promotes the formation of a multistage porous structure, which strengthens the synergistic effect between the Cu and Ce catalysts and changes the redox property of the overall catalyst. On the one hand, the strong synergy between CuO and CeO_2 adjusts the dispersion and chemical state of copper nanoparticles. On the other hand, the oxygen vacancies generated locate at the copper-cerium interface enhance the ability of oxygen storage and oxygen release of the catalyst.

ARTICLE HISTORY
Received 20 October 2019
Revised 27 December 2019
Accepted 4 February 2020

KEYWORDS
$CuCe_{0.75}Zr_{0.25}O_y$ catalyst; carbon monoxide; self-sustained combustion; pore-forming way

Introduction

With the rapid development of industry and transportation, the pollution of the atmospheric environment by the consumption of fossil fuels has become increasingly serious. In the metallurgical industry, a large amount of carbon monoxide gas, which is colorless, odorless and toxic, is produced and can bind with hemoglobin in the human body, thus endangering human health and causing death in serious cases. To control carbon monoxide emissions in industrial production, burners are usually used to ignite and dissipate it directly, which not only causes serious energy waste and environmental pollution but also

CONTACT Xiaolin Wei xlwei@imech.ac.cn State Key Laboratory of High-Temperature Gas Dynamics, Institute of Mechanics, Chinese Academy of Sciences, Beijing 100190, PR China; Baojuan Dou binfeng@imech.ac.cn College of Chemical Engineering & Materials Science, Tianjin University of Science & Technology, Tianjin, PR China

has certain dangers. Carbon monoxide catalytic combustion, which can effectively eliminate CO, has become one of the research hotspots in the field of catalytic oxidation. In order to preserve the chemical heat that may be released, Previous study in our research group demonstrated that self-sustained catalytic combustion can be achieved under high concentration of CO through the exothermic reaction of CO → CO_2 that occurs on the catalyst surface. The advantage is that once the combustion starts, the reaction can rely on the heat released by the reaction to maintain the combustion, without the need for external heat to achieve a self-sustaining combustion state, and it is a flameless combustion that occurs on the catalyst surface, with no possibility of explosion. With respect to the technology of CO combustion, the catalysts used are mainly noble metal catalysts and transition metal oxide catalysts, among which the noble metals have high cost and poor stability. Thus, the focus of research is to develop transition metal catalysts with excellent stability and low-temperature activity. Among them, the excellent catalytic effect of the Cu-Ce-Zr composite catalyst on the CO oxidation process has aroused an increase in research about chemical industry. CuO is the main active species of the CO catalytic reaction and provides active adsorption sites for CO. CeO_2 acts as an auxiliary agent, and its unique fluorite structure can effectively promote the dispersion of Cu species. In addition, ZrO_2 easily enters the CeO_2 lattice to form a Ce-Zr-O solid solution, so doping a small amount of ZrO_2 in the catalyst generates more oxygen vacancies and improves its oxygen storage capacity and thermal stability (Kuo et al. 2014).

There is no denying that the structure and activity of catalysts are influenced by preparation methods. If the catalyst has excellent porous channels, these channels can improve the diffusion and transfer capacity of the reactant molecules and products (Rivas et al. 2013, He et al. 2015a). Bacterial cellulose (BC) is widely used as a carrier or template for the synthesis of various inorganic nanostructured materials due to its special structural properties; for example, the use of a bacterial cellulose fine mesh structure provides high specific surface area and good hydrophilic properties as a pore former for preparing a composite metal oxide catalyst to degrade toluene (Kang et al. 2018a). In the Heck reaction, a Pd/BC catalyst was prepared by loading Pd with BC nanofibers (Zhou et al. 2012).

In this paper, the effects of $CuCe_{0.75}Zr_{0.25}O_y$ catalysts prepared by a sol-gel method via three different pore-forming agents (oxalic acid, cellulose and thermal decomposition) were investigated for CO self-sustained combustion. Additionally, characterization methods were used to obtain the structural properties of catalysts.

Experiment specifications

Catalyst preparation

$CuCe_{0.75}Zr_{0.25}O_y$ catalysts were manufactured using three different pore-forming agents, namely thermal decomposition, oxalic acid and cellulose method.

Thermal decomposition method

$Cu(NO_3)_2.3H_2O$, $Ce(NO_3)_3 \cdot 6H_2O$ and $Zr(NO_3)_4 \cdot 5H_2O$ in a Cu:Ce:Zr molar ratio of 4:3:1 were dissolved in 400 ml ethanol at 50 °C. After being dissolved, the temperature was raised to 80°C with stirring until the gel was formed. The gel was aged at room temperature for 48 h,

dried for 12 h at 80°C in an oven, and finally calcined at 550°C for 2 h by temperature-programmed calcination. The catalyst was pelleted and recorded as $CuCe_{0.75}Zr_{0.25}O_y$-T.

Oxalic acid method

Based on the same Cu:Ce:Zr molar ratio to thermal decomposition method, $Cu(NO_3)_2 \cdot 3H_2O$, $Ce(NO_3)_3 \cdot 6H_2O$ and $Zr(NO_3)_4 \cdot 5H_2O$ were dissolved in 400 mL ethanol at 50°C. Next, 0.24 mol/L of oxalic acid solution, used as the pore forming agent, was quickly poured into the above nitrate solution and stirred until the gel was formed. After the gel was aged at room temperature for 48 h, it was dried in an oven at 80°C for 12 hours, and calcined for 2 h by program heating to 550°C. Afterward, it was pressed to make pellets, and the catalyst was named $CuCe_{0.75}Zr_{0.25}O_y$ -O.

Cellulose method

The $Cu(NO_3)_2 \cdot 3H_2O$, $Ce(NO_3)_2 \cdot 6H_2O$ and $Zr(NO_3)_4 \cdot 5H_2O$ was dissolved at 50°C in 400 mL of absolute ethanol. 5g of bacterial cellulose is poured into the nitrate solution as a pore-forming agent, while being rapidly stirred until a gel is formed. The gel was aged for 48 h at room temperature. Then, the gel was dried in an oven at 80°C for 12 h. Next, it was calcined at a temperature of 550°C for 2 h and pelletized to obtain the $CuCe_{0.75}Zr_{0.25}O_y$ catalyst that was recorded as $CuCe_{0.75}Zr_{0.25}O_y$-C.

Characterizations

The texture properties of the catalyst were determined with an ASAP 2420 physical adsorption instrument. The mass of the sample was 0.5 g before the test, and the oxidation sample was vacuum degassed at 150°C for 12 h. During the test, the sample was cooled to −196°C in liquid nitrogen for low-temperature N_2 adsorption and desorption experiments, and the data acquisition was automatically performed by a computer. The specific surface area was calculated using the Brunauer-Emmett-Teller (BET) method with ASiQwin software. Based on the Kelvin equation, the pore size distribution curve was calculated using the Barrett-Joyner-Halenda (BJH) method.

The crystal structure of the catalyst was characterized by X-ray diffraction (XRD), which was measured by a DX-2700 X-ray diffractometer with a CuKα (λ = 0.1541 nm). The voltage and current of the X-ray tube were 40 kV and 30 mA, respectively. The scanning step was 0.06°, the angle range was 5–85°, and the scanning rate was 2°/min.

Raman characterizes the position of the vibration peak and the oxygen vacancy concentration in the catalyst. Raman characterization was performed on a HORIBA LabRAM HR Evolution laser confocal micro-Raman spectrometer. The device was equipped with a 488 nm laser, a high-speed grating feedback platform (HSES) of 100 nm steps, a travel range of 112 mm×76 mm, a spectral range of 10 to 9000 cm^{-1}, and a resolution of 1 cm^{-1}. The tip of the detector was adjusted to a distance of 2 mm from the sample to scan the sample that was placed on a glass slide in a dark environment, and then the chart data was saved.

X-ray photoelectron spectroscopy (XPS) was used to determine the composition of the catalyst surface and the valence states of each element. The energy spectrum data were measured with a Perkin-Elmer PHI-1600 ESCA X-ray photoelectron spectrometer. The

X-ray source was a Mg anode target (350 eV). The binding energy values of each species were corrected by C 1s (Eb = 284.8 eV) as an internal standard.

The reducibility of the catalyst was characterized by a temperature-programmed reduction of H_2 (H_2-TPR). H_2-TPR analysis was performed using a PCA-140 instrument. 0.1 g of catalyst was filled in a U-shaped quartz tube, pretreated with carrier gas (Ar gas) and heated from room temperature to 500°C at 20°C/min for 1 h. After lowering the temperature to room temperature, it was reduced with 5% H_2/Ar. The flow rate was set to 50 mL/min, the sample was heated from 30°C to 800°C with a heating rate of 10°C/min. Then, the peak signal was detected by a TCD.

Characterization of oxygen species in the catalysts was obtained by a temperature-programmed desorption of oxygen (O_2-TPD). O_2-TPD analysis was recorded on the same instrument as the H_2-TPR. 0.2 g of the fresh catalyst samples were adsorbed by O_2 at room temperature under an O_2 atmosphere (50 mL/min) for 1h. Then, the atmosphere was switched to Ar at a flow rate of 50 mL/min, and the reaction temperature was raised to 1000°C at a rate of 10°C/min. Finally, the peak signal was detected by TCD.

Catalytic activity *testing*

To measure catalyst activity, catalyst samples (0.2 g, 0.1–0.15 mm) were packed in a micro-fixed-bed quartz tube reactor (4 mm inner diameter) with a temperature control device (FCD-13AS/M, Shinko, Japan). Pure CO gas, O_2 gas and N_2 gas were adjusted by three mass flowmeter, and a stable concentration mixture was prepared by a mixer. The mixed reaction gas concentration was controlled to 3% CO+5% O_2, N_2 as balance, and the total gas flow rate was 0.2 L/min. After the gas path was stabilized, the gas was fed into a fixed-bed reactor for the catalytic reaction and the concentration of each component of the inlet and outlet gases of the reactor were analyzed online by an infrared gas analyzer. Then, the conversion rate of CO was calculated. The activity of the catalyst is expressed by the conversion of CO. The formula for calculating the conversion is as follows (1–1):

$$Con.(\%) = \frac{c_{in} - c_{out}}{c_{in}} \times 100\% \qquad (1-1)$$

where *Con.* is the conversion rate of CO, %, and C_{in} and C_{out} are the concentration of CO at the inlet and outlet of the reactor, respectively.

Results and discussion

Catalyst textural properties

Figure 1a and 1b display the N_2 physical adsorption-desorption isotherms and corresponding pore size distribution curves of $CuCe_{0.75}Zr_{0.25}O_y$-T, $CuCe_{0.75}Zr_{0.25}O_y$-O and $CuCe_{0.75}Zr_{0.25}O_y$-C catalysts, respectively, with the the textural properties of the $CuCe_{0.75}Zr_{0.25}O_y$ catalysts listed in Table 1. The isothermal adsorption-desorption curves of the three catalysts all have the characteristics of type IV isotherms with an H3-type hysteresis loop at a relative pressure (P/P_0) range of 0.4 to 1.0 (Xie et al. 2018). The above results indicate the presence of mesopores in the catalysts. Formation of worm-like mesopores in the $CuCe_{0.75}Zr_{0.25}O_y$-T catalyst was obtained through the analysis of the catalyst exhibiting typical type IV adsorption isotherms and a steep capillary

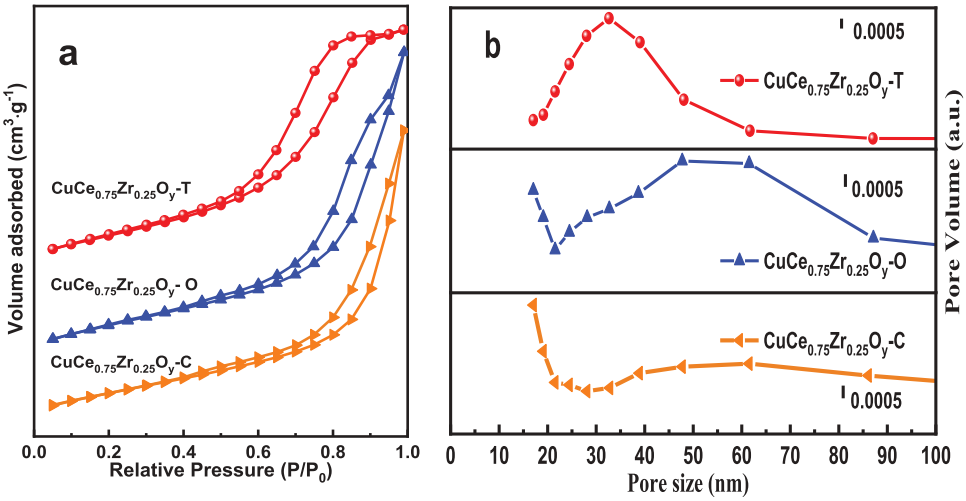

Figure 1. N_2 adsorption/desorption isotherms (a) and pore size distributions (b) of the $CuCe_{0.75}Zr_{0.25}O_y$ catalysts.

Table 1. Textural properties of the $CuCe_{0.75}Zr_{0.25}O_y$ catalysts.

Samples	Surface area ($m^2 \cdot g^{-1}$)	Mean pore size (nm)	Pore volume ($cm^3 \cdot g^{-1}$)
$CuCe_{0.75}Zr_{0.25}O_y$-T	30.31	3.83	0.074
$CuCe_{0.75}Zr_{0.25}O_y$-O	32.08	5.77	0.084
$CuCe_{0.75}Zr_{0.25}O_y$-C	35.54	8.64	0.105

condensation step with an H2-type hysteresis loop at a relative pressure (P/P_0) range of 0.5 to 1.0. It is known from the catalyst pore size distribution diagram shown in Figure 1b that the catalyst has mesoporous structures of different sizes. The surface area and pore volume of the $CuCe_{0.75}Zr_{0.25}O_y$-T (30.31 $m^2 \cdot g^{-1}$, 0.074 $cm^3 \cdot g^{-1}$) are lower than others, while those of the $CuCe_{0.75}Zr_{0.25}O_y$-C (35.54 $m^2 \cdot g^{-1}$,0.105 $cm^3 \cdot g^{-1}$) are highest among others. The pore size distribution of the $CuCe_{0.75}Zr_{0.25}O_y$-O and $CuCe_{0.75}Zr_{0.25}O_y$-C catalysts is approximately the same value, and hence it is evident that the pore former is responsible for the pore size distribution of the catalysts.

Crystal structure of the catalysts

The XRD patterns of the $CuCe_{0.75}Zr_{0.25}O_y$–T, $CuCe_{0.75}Zr_{0.25}O_y$–O and $CuCe_{0.75}Zr_{0.25}O_y$–C catalysts are presented in Figure 2. Two weak characteristic diffraction peaks appear in the three catalyst samples at $2\theta = 35.9°$ and 39.1°, which are attributed to copper oxides and indicate that bulk CuO microcrystals are formed on the catalyst surface (Kang et al. 2018a). Typical CeO_2 diffraction peaks that are characteristic of a fluorite structure appear at 28.5°, 47.4°, 56.5° (Liu et al. 2010). Compared with pure CeO_2, the three catalysts retain the CeO_2 fluorite structure. The calculated lattice parameters of CeO_2 in the three catalysts were 0.539 nm, 0.535 nm and 0.534 nm, all of which were smaller than that of the pure CeO_2 (0.5412 nm). This was due to the partial Zr^{4+} (0.074 nm) and Cu^{2+} (0.073 nm) entering the CeO_2 lattice, which partially replaces the Ce^{4+} to form new solid solutions and causes crystal lattice distortion of CeO_2. The lattice distortion of CeO_2 can enhance

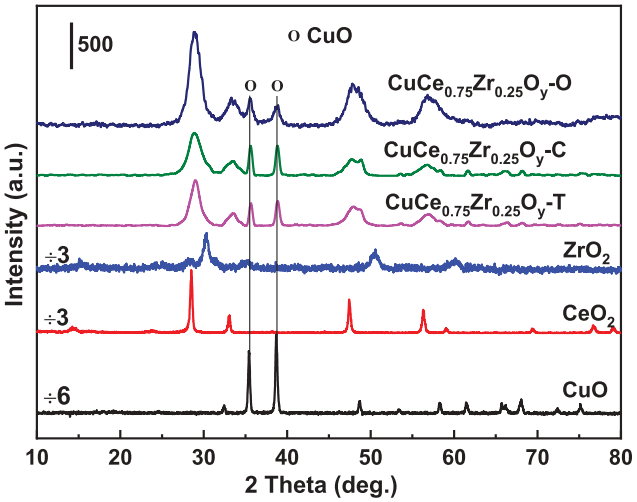

Figure 2. XRD patterns of the different $CuCe_{0.75}Zr_{0.25}O_y$ catalysts.

the oxygen species adsorption capacity of the catalyst and is beneficial for increasing the activity of the catalyst (Luo et al. 2007).

Catalyst oxygen species and oxygen vacancy concentration

O_2-TPD measurements were used to examine the adsorption of oxygen on the $CuCe_{0.75}Zr_{0.25}O_y$–T, $CuCe_{0.75}Zr_{0.25}O_y$–O and $CuCe_{0.75}Zr_{0.25}O_y$–C catalysts. The difficulty of changing the oxygen species of the catalyst is $O_2 \rightarrow O_2^- \rightarrow O^- \rightarrow O_2^-$(physisorbed oxygen O_2, chemisorbed oxygen $O_2^-$and O^-, lattice oxygen O_2^-). As shown in Figure 3, the oxygen desorption peak of all catalysts can be divided into a low-temperature peak (50–300°C) is related to the weakly

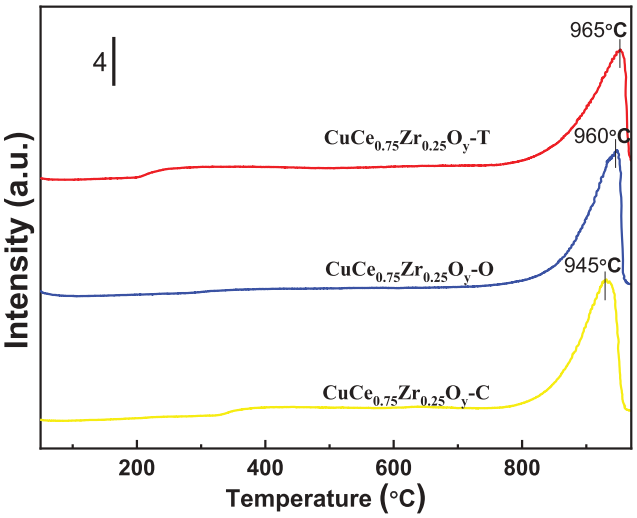

Figure 3. O_2-TPD profiles of the different $CuCe_{0.75}Zr_{0.25}O_y$ catalysts.

adsorbed oxygen (O_2), an intermediate-temperature peak (300–600°C) is due to the chemisorbed surface-active oxygen (O_2^-/O^-), and a high-temperature peak (600–1100°C) related to the lattice oxygen (O_2^-) bonded to the metal cations (Zheng et al. 2016). It can also be seen from Figure 3 that the $CuCe_{0.75}Zr_{0.25}O_y$-C catalyst appeared as a desorption peak of lattice oxygen at 945°C, and the $CuCe_{0.75}Zr_{0.25}O_y$-T catalyst started the desorption of lattice oxygen at approximately 965°C. Previous study in our group showed that the CO is adsorbed on the active center of the catalyst surface firstly, and then reacted with lattice oxygen to produce gas phase CO_2, leaving oxygen vacancy and completes the cycle by converting O_2 into lattice oxygen (Kang et al. 2018b). Compared with the $CuCe_{0.75}Zr_{0.25}O_y$-T and $CuCe_{0.75}Zr_{0.25}O_y$-O catalysts, the $CuCe_{0.75}Zr_{0.25}O_y$-C catalyst is most prone to lattice oxygen desorption. This is also one of the reasons for the $CuCe_{0.75}Zr_{0.25}O_y$-C catalyst exhibiting the highest activity among the three catalysts.

The Raman spectrum and oxygen vacancy concentration of the $CuCe_{0.75}Zr_{0.25}O_y$–T, $CuCe_{0.75}Zr_{0.25}O_y$–O and $CuCe_{0.75}Zr_{0.25}O_y$–C catalyst are shown in Figure 4. It can be seen from Figure 4 that there are four diffraction peaks in the Raman spectrum of the catalyst: the peak at 290 cm^{-1} is the Raman peak of CuO (He et al. 2014); the 463 cm^{-1} peak is a triple vibration peak attributed to the oxygen atom around Ce^{4+} (F_{2g}), the broad peak at 628 cm^{-1} is attributable to an oxygen vacancy (O_v) generated by the formation of Ce^{3+} in the CeO_2 lattice defect (Rivas et al. 2011a), and the peak at 1188 cm^{-1} is attributed to a vibrational peak of the asymmetric structure of CeO_2 . The oxygen vacancy concentration of the catalyst is defined as the ratio between the peak area (628 cm^{-1}) of the oxygen vacancy O_v and the peak area (463 cm^{-1}) of the asymmetric vibration peak F_{2g} (Kim et al. 2007). The A_{628}/A_{463} value of the $CuCe_{0.75}Zr_{0.25}O_y$-C catalyst is 0.349, which is higher than the $CuCe_{0.75}Zr_{0.25}O_y$-O catalyst (A_{628}/A_{463} = 0.29) and the $CuCe_{0.75}Zr_{0.25}O_y$-T catalyst (A_{628}/A_{463} = 0.26), and therefore the $CuCe_{0.75}Zr_{0.25}O_y$-C catalyst exhibits the largest oxygen vacancy concentration. Thus, the chosen pore former has a significant influence on the oxygen vacancy concentration of catalysts.

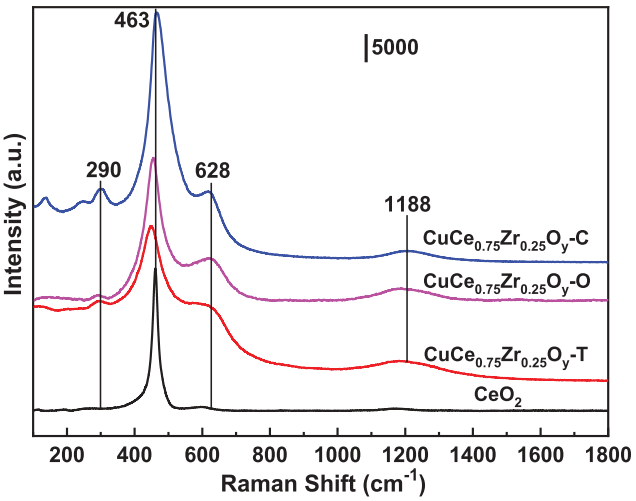

Figure 4. Raman spectra of the different $CuCe_{0.75}Zr_{0.25}O_y$ catalysts.

There are two forms of copper species (Cu^{+} and Cu^{2+}) in the copper-cerium catalyst system, and the active site that provide active oxygen and the sites for CO adsorption/activation that participate in CO combustion has been considered to be located at the copper-cerium interface, Cu^{+} atoms direct bonding in the oxygen vacancy of cerium form Cu^{+}-[O_v]-Ce^{3+} (Chen et al. 2019), Under oxygen-rich or oxidation conditions, The adsorption of one oxygen to the oxygen vacancy will cause two Cu^{+} atomes to become Cu^{2+},which converts Cu^{+}-[O_v]- to Cu^{2+}-[O^{2-}]-. Therefore, the combination of CeO_{2-x} and CeO_2 can easily interconvert (Cu-O_v-Ce ↔ Cu-O-Ce) under different reaction atmospheres, having that combination accelerates the reaction cycle and enhances the catalytic activity (Yu, Gao, Dong 2012). The increased oxygen vacancies of the $CuCe_{0.75}Zr_{0.25}O_y$-C catalyst are beneficial to the catalytic reaction of CO.

Temperature-programmed hydrogen reduction analysis

The H_2-TPR characterization results of the $CuCe_{0.75}Zr_{0.25}O_y$–T, $CuCe_{0.75}Zr_{0.25}O_y$–O and $CuCe_{0.75}Zr_{0.25}O_y$–C catalysts are displayed in Figure 5. The reduction peak of the catalyst can be divided into four reduction peaks of α, β and γ, but the reducibility of the $CuCe_{0.75}Zr_{0.25}O_y$ catalyst prepared by different pore-forming agents is quite different. The α peak at approximately 160°C is attributed to the reduction peak of Cu^{2+} entering the CeO_2 lattice. The β peak near 270°C is the reduction peak of the CuO, which is highly dispersed on the surface of the catalyst. (Lu et al. 2013, Rivas et al. 2011b),The γ peak that is higher than 300°C may be a reduction peak of other oxides, such as clusters of CuO or solid solution of Ce-Zr-O_y (Su et al. 2011; Zhu et al. 2015). The characterization results confirm the presence of Cu^{2+} in the CeO_2 lattice, which are consistent with the XRD characterization results.

Table 2 provides evidence that the $CuCe_{0.75}Zr_{0.25}O_y$-T catalyst has the lowest hydrogen consumption than the catalysts with other pore formers. Therefore, the $CuCe_{0.75}Zr_{0.25}O_y$-T catalyst exhibits a poor reducibility. Compared with the reduction peak position of

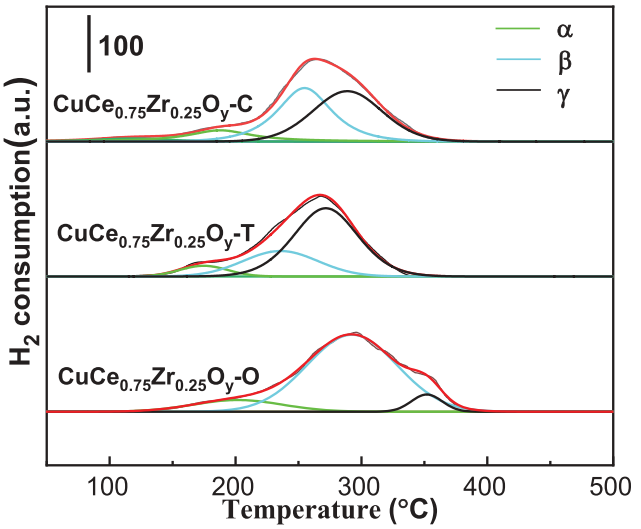

Figure 5. H_2-TPR profiles of the different $CuCe_{0.75}Zr_{0.25}O_y$ catalysts.

Table 2. H_2 consumptions of the different $CuCe_{0.75}Zr_{0.25}O_y$ catalysts.

	H_2 consumption ($\mu mol \cdot g^{-1}$)			
Samples	α peak	β peak	γ peak	Total
$CuCe_{0.75}Zr_{0.25}O_y$-C	239	662	607	1508
$CuCe_{0.75}Zr_{0.25}O_y$-T	91	353	832	1276
$CuCe_{0.75}Zr_{0.25}O_y$-O	146	1275	158	1579

$CuCe_{0.75}Zr_{0.25}O_y$-O, those of $CuCe_{0.75}Zr_{0.25}O_y$-C shift toward lower temperatures, due to the strong synergy amid CuO and CeO_2, the Cu-O-Ce junction exists in the solid solution of Cu-Ce-Zr, which may reduce the redox potential of the copper species. Therefore, the strong synergy between CuO and CeO_2 enhances the low-temperature reductive properties of the $CuCe_{0.75}Zr_{0.25}O_y$-C catalyst.

XPS analysis

The chemical states of the $CuCe_{0.75}Zr_{0.25}O_y$–T, $CuCe_{0.75}Zr_{0.25}O_y$–O and $CuCe_{0.75}Zr_{0.25}O_y$–C catalysts can be analyzed by XPS. The Cu 2p spectrum of the $CuCe_{0.75}Zr_{0.25}O_y$ catalyst (Figure 6) shows a vibration peak located in the range of 938.1 eV~947.7 eV, which confirms the existence of Cu^{2+}, as shown in Figure 6a. After deconvolution and fitting of the Cu $2p_{3/2}$ peak, the Cu $2p_{3/2}$ peak can be split into two peaks at 932.6 eV and 934.4 eV, corresponding to Cu^+ (Cu_2O) and Cu^{2+} (CuO) ions, respectively. The Ce 3d spectrum of the catalysts (Figure 6b) that shows eight diffraction peaks for all three catalysts tested: two diffraction peaks appearing at 882.6 eV and 901.1 eV represent characteristic peaks of the two spin orbitals Ce $3d_{5/2}$ and Ce $3d_{3/2}$, four strong peaks of the $CuCe_{0.75}Zr_{0.25}O_y$ catalyst (882.6, 899.4, 901.1, and 917.1 eV) and two smaller peaks (889.4 and 907.7 eV) are able to be ascribed to different Ce 4f electron rows in the final Ce^{4+} species, and the weakest two peaks (884.8 and 903.2 eV) each represent one of two possible electronic arrangements of the final Ce^{3+} species (Chen et al. 2009). The chemical valence of cerium is mainly in the +4 oxidation state, and a small amount of cerium is in the +3 oxidation state. Since Ce^{4+} is replaced by Zr^{4+} during calcination, the cerium and zirconium atoms are more uniformly distributed on the catalyst surface, which promotes a valence change of $Ce^{4+} \rightarrow Ce^{3+}$ (He et al. 2015b). Among the O 1s spectra of the catalysts, the O 1s peak with a binding energy of 527.8 ~ 530.3 eV belongs to surface lattice oxygen (OI), the O 1s peak of 530.6 ~ 531.1 eV belongs to surface oxygen (OII), and the O 1s peak of 532.1 ~ 534.3 eV belongs to the adsorption of oxygen (OIII) (Tang et al. 2015). It can be gathered from the Table 3 that the surface copper and cerium contents of the $CuCe_{0.75}Zr_{0.25}O_y$-C catalyst are smaller than that of the other two catalysts, indicating that the bacterial cellulose pore former enhances the metal-support interactions of Cu and Ce in the $CuCe_{0.75}Zr_{0.25}O_y$-C catalyst.

Catalyst activity

Figure 7 shows the results for the individual thermal catalytic removal of 3% CO to evaluate the activity of the $CuCe_{0.75}Zr_{0.25}O_y$–T, $CuCe_{0.75}Zr_{0.25}O_y$–O and $CuCe_{0.75}Zr_{0.25}O_y$–C catalysts. Different pore formers have a significant influence on the thermal catalytic activity of the catalysts. The CO removal rates of the three $CuCe_{0.75}Zr_{0.25}O_y$ catalysts were less than 5% before 60°C. As the reaction temperature increased, the $CuCe_{0.75}Zr_{0.25}O_y$-C catalyst showed better CO catalytic activity than that of the other two catalysts. Under the condition of

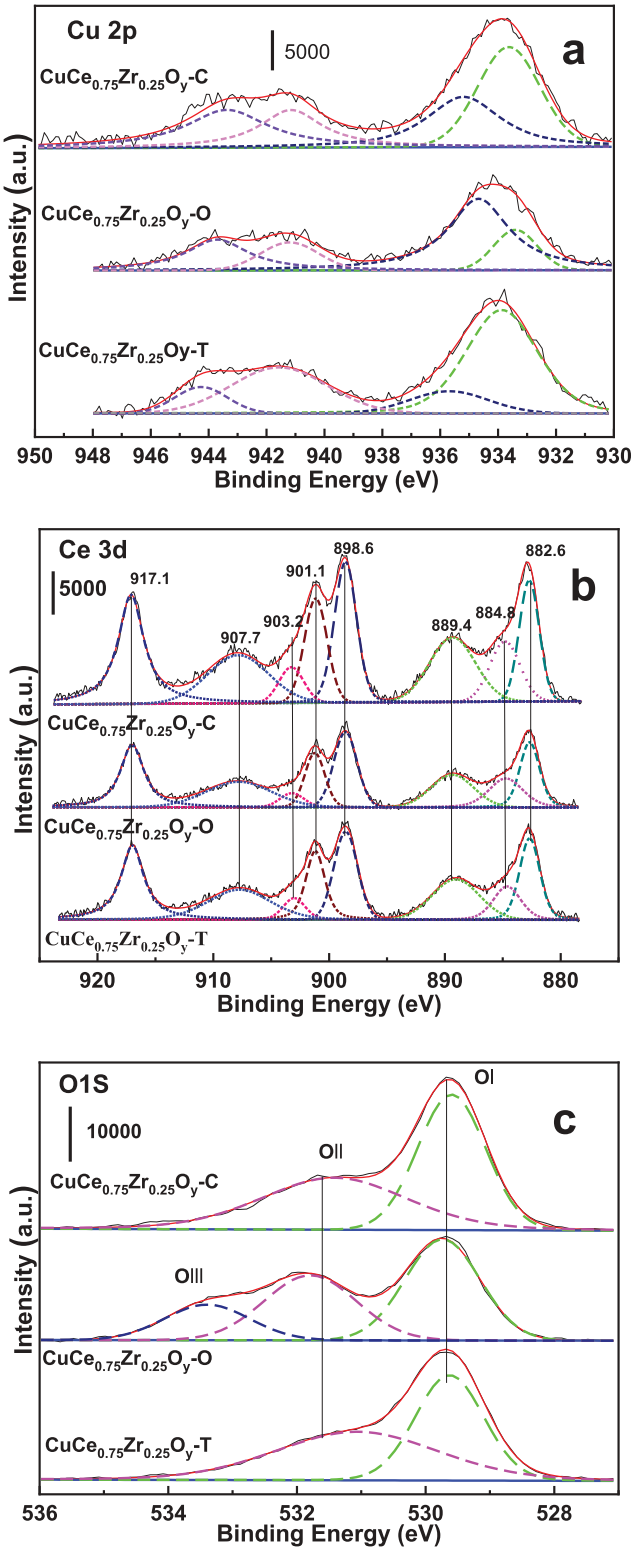

Figure 6. XPS spectra of the $CuCe_{0.75}Zr_{0.25}O_y$ catalysts: (a) Cu 2p, (b) Ce 3d, and (c) O 1s.

Table 3. Surface species of the $CuCe_{0.75}Zr_{0.25}O_y$ catalysts.

Samples	Cu (at.%)	Ce (at.%)	Zr (at.%)
$CuCe_{0.75}Zr_{0.25}O_y$-T	36.1	47.4	16.5
$CuCe_{0.75}Zr_{0.25}O_y$-O	37.87	46.25	15.88
$CuCe_{0.75}Zr_{0.25}O_y$-C	35.5	45.72	18.78

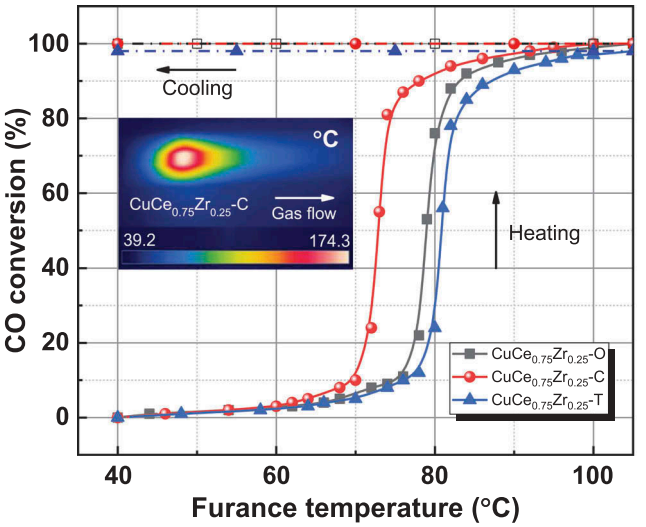

Figure 7. Catalytic activities of the different $CuCe_{0.75}Zr_{0.25}O_y$ catalysts for CO conversion.

a reaction gas (3% CO+5%O_2/N_2), the T_{10}(70°C), T_{50} (73°C) and T_{90} (78°C) of the $CuCe_{0.75}Zr_{0.25}O_y$-C catalyst were obviously lower than those of the other catalysts. The above characterization results show that CeO_2 and CuO in the $CuCe_{0.75}Zr_{0.25}O_y$-C catalyst create a strong synergy and high oxygen vacancy concentration, which are the main reasons for the catalyst's optimal activity. The strong synergistic effect between CeO_2 and CuO makes the $CuCe_{0.75}Zr_{0.25}O_y$-C catalyst have good low-temperature reducibility. The high oxygen vacancy concentration is beneficial for adsorbing oxygen species, thus forming more active oxygen and increasing the activity of the catalyst (Kima, Nama, Chunga 1994).

Conclusion

The effects of a series of $CuCe_{0.75}Zr_{0.25}O_y$ catalysts manufactured by a sol-gel method via three different pore-forming agents (oxalic acid, cellulose and thermal decomposition) were investigated for CO self-sustained combustion, and the main conclusions are as follows.

The results obtained show that the $CuCe_{0.75}Zr_{0.25}O_y$ catalyst prepared by cellulose as a sol-gel pore-forming agent exhibits the highest activity among the three catalysts. Under the condition of a reaction gas (3%CO+5%O_2/N_2), the T_{10} (70°C), T_{50} (73°C) and T_{90} (78°C) of the catalyst from cellulose are obviously lower than those of the other catalysts. Experiments show that different pore-forming agents have obvious effects on the structure and properties of the catalysts and the catalytic oxidation of CO. The cellulose pore-forming agent promotes the formation of a multistage porous structure, which strengthens the synergistic effect between the Cu and Ce in

the catalyst and changes the redox property of the overall catalyst. Strong metal-support between CuO and CeO_2 adjusts the dispersion and chemical state of copper nanoparticles. The oxygen vacancies generated at the copper-cerium interface enhance the ability of oxygen storage and oxygen release of the catalyst. Moreover, all of the above factors promote the catalytic reaction and improve the efficiency of catalytic reaction.

Acknowledgments

This work is financially supported by the National Natural Science Foundation of China (51776216, 51736010). The work is also supported by Dalian National Laboratory for Clean Energy, Dalian 116023, China and the Transformational Technologies for Clean Energy and Demonstration, Strategic Priority Research Program of the Chinese Academy of Sciences, Grant No.XDA21040500.

Funding

This work was supported by the National Natural Science Foundation of China [51736010,51776216] and the Transformational Technologies for Clean Energy and Demonstration, Strategic Priority Research Program of the Chinese Academy of Sciences,Grant No.XDA21040500.

References

Chen, A., X. J. Yu, Z. Yan, S. Miao, Y. Li, and S. Kuld. 2019. Structure of the catalytically active copper–ceria interfacial perimeter. *Nat. Catal.* 2:334-341.

Chen, H. L., H. M. Lee, S. H. Chen, and M. B. Chang. 2009. Removal of volatile organic compounds by single-stage and two-stage plasma catalysis systems: A review of the performance enhancement mechanisms, current status, and suitable applications. *Environ. Sci. Technol.* 43 (7):2216–27.

He, C., B. T. Xu, J. W. Shi, N. L. Qiao, Z. P. Hao, and J. L. Zhao. 2015a. Catalytic destruction of chlorobenzene over mesoporous $ACeO_x$ (A = Co, Cu, Fe, Mn, or Zr) composites prepared by inorganic metal precursor spontaneous precipitation. *Fuel Process. Tech.* 130:179–87.

He, C., Y. K. Yu, J. W. Shi, Q. Shen, J. S. Chen, and H. X. Liu. 2015b. Mesostructured Cu–Mn–Ce–O composites with homogeneous bulk composition for chlorobenzene removal: Catalytic performance and microactivation course. *Mater. Chem. Phys.* 157:87–100.

He, C., Y. K. Yu, L. Yue, N. L. Qiao, J. J. Li, Q. Shen, W. J. Yu, J. S. Chen, and Z. P. Hao. 2014. Low-temperature removal of toluene and propanal over highly active mesoporous $CuCeO_x$ catalysts synthesized via a simple self-precipitation protocol. *Appl. Catal. B* 147:156–66.

Kang, R. N., X. L. Wei, F. Bin, Z. B. Wang, Q. L. Hao, and B. J. Dou. 2018a. Reaction mechanism and kinetics of co oxidation over a $CuO/Ce_{0.75}Zr_{0.25}O_{2-\delta}$, catalyst. *Appl. Catal. A* S0926860X1830365X. 565:46-58.

Kang, R. N., X. L. Wei, H. X. Li, and F. Bin. 2018b. Sol-gel enhanced mesoporous Cu-Ce-Zr catalyst for toluene oxidation. *Combust. Sci. Technol.* 190 (5):878–92.

Kim, H. H., S. Tsubota, M. Daté, A. Ogata, and S. Futamura. 2007. Catalyst regeneration and activity enhance-ment of Au/TiO_2 by atmospheric pressure nonthermal plasma. *Appl. Catal. A* 329 (10):93–98.

Kima, K. D., I. S. Nama, and J. S. Chunga. 1994. Supported $PdCl_2$ -$CuCl_2$ catalysts for carbon monoxide oxidation 1. Effects of catalyst composition and reaction conditions. *Appl. Catal. B* 5 (1–2):103–15.

Kuo, C. P., H. T. Liao, C. C. K. Chou, and C. F. Wu. 2014. Source apportionment of particulate matter and selected volatile organic compounds with multiple time resolution data. *Sci. Total. Environ.* 472:880–87.

Liu, L., Z. Yao, B. Liu, and Dong. 2010. Correlation of structural characteristics with catalytic performance of $CuO/Ce_XZr_{1-X}O_2$, catalysts for NO reduction by CO. *J. Catal.* 275 (1):45–60.

Lu, H. F., Y. Zhou, W. F. Han, and Y. F. Chen. 2013. Promoting effect of ZrO_2 carrier on activity and thermal stability of CeO_2-based oxides catalysts for toluene combustion. *Appl. Catal. A* 464–465:101–08.

Luo, M. F., J. M. Ma, J. Q. Lu, Y. P. Song, and Y. J. Wang. 2007. High-surface area CuO–CeO_2 catalysts prepared by a surfactant-templated method for low-temperature CO oxidation. *J. Catal.* 246:52–59.

Rivas, B. D., R. López-Fonseca, M. Á. Gutiérrez-Ortiz, and J. I. Gutiérrez-Ortiz. 2011a. Combustion of chlorinated VOCs using K-$CeZrO_4$ catalysts. *Catal.Today* 176 (1):470–73.

Rivas, B. D., R. López-Fonseca, M. Á. Gutiérrez-Ortiz, and J. I. Gutiérrez-Ortiz. 2011b. Impact of induced chlorine-poisoning on the catalytic behaviour of $Ce_{0.5}Zr_{0.5}O_2$ and $Ce_{0.15}Zr_{0.85}O_2$ in the gas-phase oxidation of chlorinated VOCs. *Appl. Catal. B* 104:373–81.

Rivas, B. D., C. Sampedro, M. García-Real, R. López-FonsecA, and J. I. Gutiérrez-Ortiz. 2013. Promoted activity of sulphated Ce/Zr mixed oxides for chlorinated VOC oxidative abatement. *Appl. Catal. B* 90:225–35.

Su, Y., D. H. Wang, S. P. Bai, J. Jia, Y. Qin, and J. S. Jin. 2011. Study on Catalytic Oxidation of Carbon Monoxide by Low Temperature Plasma with Catalyst. *Speci. Petrochemicals* 28 (4):27–31.

Tang, W. X., X. F. Wu, G. Liu, S. D. Li, D. Y. Li, W. H. Li, and Y. F. Chen. 2015. Preparation of hierarchical layer-stacking Mn-Ce composite oxide for catalytic total oxidation of VOCs. *J. Rare Earth* 33:62–69.

Xie, Y., J. F. Wu, G. J. Jing, H. Zhang, S. H. Zeng, and X. P. Tian. 2018. Structural origin of high catalytic activity for preferential CO oxidation over CuO/CeO_2 nanocatalysts with different shapes. *Appl. Catal. B* S092633731830804X. 239:665-676.

Yu, Q., F. Gao, and L. Dong. 2012. Recent progress of Cu-based catalysts for catalytic elimination of CO. *Chin. J. Catal.* V33 (8):1245–56.

Zheng, Y. N., K. Z. Li, H. Wang, Y. Wang, D. Tian, and Y. Wei. 2016. Structure dependence and reaction mechanism of CO oxidation: A model study on macroporous CeO_2 and CeO_2-ZrO_2 catalysts. *J. Catal.* 344:365–77.

Zhou, P., H. Wang, J. Yang, J. Tang, D. Sun, and W. Tang. 2012. Bacteria cellulose nanofibers supported palladium(0) nanocomposite and its catalysis evaluation in heck reaction. *Ind. Eng. Ches. Res.* 51 (16):5743–48.

Zhu, X., X. Gao, R. Qin, Y. Zeng, R. Qu, and C. Zheng. 2015. Plasma-catalytic removal of formaldehyde over Cu-Ce catalysts in a dielectric barrier discharge reactor. *Appl. Catal. B* 170:293–300.